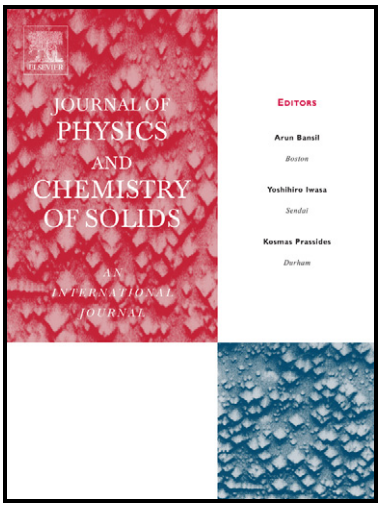

www.elsevier.com/locate/jpcs

First-principles calculations of electronic, optical and elastic properties of $ZnAl_2S_4$ and $ZnGa_2O_4$

M.G. Brik

PII: S0022-3697(10)00208-8
DOI: doi:10.1016/j.jpcs.2010.07.007
Reference: PCS 6214

To appear in: *Journal of Physics and Chemistry of Solids*

Received date: 2 February 2010
Revised date: 9 April 2010
Accepted date: 7 July 2010

Cite this article as: M.G. Brik, First-principles calculations of electronic, optical and elastic properties of $ZnAl_2S_4$ and $ZnGa_2O_4$, *Journal of Physics and Chemistry of Solids*, doi:10.1016/j.jpcs.2010.07.007

First-principles calculations of electronic, optical and elastic properties of $ZnAl_2S_4$ and $ZnGa_2O_4$

M.G. Brik

Institute of Physics, University of Tartu, Riia 142, Tartu 51014, Estonia. E-mail: brik@fi.tartu.ee

Abstract

The optimized crystal structures, band structures, partial and total densities of states (DOS), dielectric functions, refractive indexes and elastic constants for $ZnAl_2S_4$ and $ZnGa_2O_4$ were calculated using the CASTEP module of Materials Studio package. Pressure effects were modeled by performing these calculations for different values of external hydrostatic pressure up to 50 GPa. Obtained dependencies of the unit cell volume on pressure were fitted by the Murnaghan equation of state, and the relative changes of different chemical bond lengths were approximated by quadratic functions of pressure. Variations of applied pressure were shown to produce considerable re-distribution of the electron densities around ions in both crystals, which is evidenced in different trends for the effective Mulliken charges of the constituting ions and changes of contour plots of the charge densities. The longitudinal and transverse sound velocities and Debye temperatures for both compounds were also estimated using the calculated elastic constants.

Key words: A. inorganic compounds; C. Ab initio calculations; D. electronic structure;

1. Introduction

A large group of compounds with spinel structure are generally described by the AB_2X_4 formula (where A and B are di- and trivalent cations, respectively, and X is a divalent anion). There are two types of cation sites in the spinel structure: tetrahedral for A species and octahedral for B species. Compounds from this family usually have wide band gaps, which can be attractive for various optical applications [1]. Wide band gap also makes these compounds suitable for doping with different impurities to get luminescence in particular spectral region. Optical properties of several impurity ions in these compounds were studied previously, e.g. Cr^{3+} in $ZnAl_2S_4$ [2–7], Fe in $ZnGa_2O_4$ [8]; Mn in $ZnGa_2O_4$ [9]; optical properties of $ZnGa_2O_4$ nanoparticles were reported in Ref. [10]. Structural and elastic properties of ZnX_2O_4 (X=Al, Ga, In) were calculated from first principles in Ref. [11].

In spite of considerable efforts on both experimental and theoretical studies of these compounds, previously reported results for the calculated properties of the bulk materials are somewhat different (comparison between the previous and present calculations will be given below). Besides, it turned out that ab initio calculations of the optical properties and careful studies of the pressure effects on the interionic distances and electron density distribution around ions in these compounds (especially $ZnAl_2S_4$) are lacking, to the best of the author's knowledge. So, this was one of motivations for the

present study, which reports the results of first-principles calculations of a wide range of physical properties for $ZnAl_2S_4$ and $ZnGa_2O_4$ single crystals. The calculated results include the optimized crystal structures (for various pressures from 0 to 50 GPa), band structures and density of states, dielectric functions and refractive indexes, elastic constants, dependencies of the chemical bond lengths and unit cell volumes on pressure, sound velocities and Debye temperatures. In addition, influence of the applied pressure on the charge density distributions, Mulliken charges, and chemical bond orders was considered.

The paper is structured as follows: in the next section the crystal structure of the considered crystals and the computational details will be described briefly, then the calculated results will be presented and compared with available experimental data and results of other calculations. The paper will be concluded with a short summary.

2. Crystal structure and computational details

Both considered crystals have a cubic crystal structure, space group Fd-3m with lattice constants (in Å) 8.3342 for $ZnGa_2O_4$ [12] and 10.009 for $ZnAl_2S_4$ [13]. There are eight formula units in one unit cell. Each Al (Ga) atom is six-fold coordinated by the S (O) ions, respectively; each Zn ion is surrounded by 4 anions (O or S). The experimental crystal structural data were taken as an initial input for optimizing the crystal structure and calculations of the electronic, optical and elastic properties, as described below.

All calculations were performed in the density functional theory (DFT) framework, using the CASTEP (Cambridge Serial Total Energy Package) module [14] of Materials Studio 4.0. The total plane-wave pseudopotential method forms a basis of the CASTEP calculations. The exchange-correlation effects were treated within the generalized gradient approximation (GGA) with the Perdew-Burke-Ernzerhof functional [15]. The Monkhorst-Pack scheme *k*-points grid sampling was set at 5×5×5 for the Brillouin zone. The plane-wave basis set energy cutoff was set at 310 eV for $ZnAl_2S_4$ and 340 eV for $ZnGa_2O_4$; ultrasoft pseudopotentials were used for all chemical elements. The convergence parameters were as follows: total energy tolerance – 1×10^{-5} eV/atom, maximum force tolerance 0.03 eV/nm, maximal stress component 0.05 GPa and maximal displacement 0.001 Å.

3. Results of calculations

3.1. Optimized crystal structures, electronic and optical properties

The optimized lattice constants are shown in Table 1, in comparison with experimental findings and results of other available calculations for $ZnGa_2O_4$. As seen from this Table, agreement between the results of the present calculations and experimental data is very good. Structural properties of

$ZnGa_2O_4$ were calculated by other authors as well (with rather wide range of the calculated lattice constants), whereas similar calculations for $ZnAl_2S_4$ are scarce.

Calculated band structures of $ZnAl_2S_4$ and $ZnGa_2O_4$ are shown in Figures 1 and 2, respectively. Coordinates of the special points of the Brillouin zone are as follows (in terms of unit vectors of the reciprocal lattice): W(0.5, 0.25, 0.75), L(0.5, 0.5, 0.5), G(0, 0, 0), X(0.5, 0, 0.5), K(0.375, 0.375, 0.750). The calculated band gaps E_g were 2.699 eV ($ZnAl_2S_4$) and 2.571 eV ($ZnGa_2O_4$), whereas the corresponding experimental values are 3.42 eV ($ZnAl_2S_4$, [18]) and 4.0 eV ($ZnGa_2O_4$, [19]). Such an underestimation of the calculated band gaps is related to well-known DFT limitations, namely not taking into account the discontinuity in the exchange-correlation potential [20], and is a common feature of all DFT calculations. In order to overcome such a discrepancy, the so called scissor operator [21] can be used. This operator produces a simple rigid shift of the unoccupied conduction band with respect to the valence band, and thus effectively eliminates the difference between the theoretical and experimental gap values. In this case the value of the scissor operator was 0.7 eV for $ZnAl_2S_4$ and 1.5 eV for $ZnGa_2O_4$. The calculated band structures in Figs. 1 and 2 are corrected with inclusion of the corresponding scissor operators. As seen from these figures, both compounds have indirect band gap, which is in agreement with previous literature data [8, 18]. However, there exists some difference in how this "indirect character" of the band gap is formed in both compounds. The top of the valence band for $ZnAl_2S_4$ is flat near the G point, whereas in $ZnGa_2O_4$ the top of the valence band and the bottom of the conduction band are simply realized at different points of the Brillouin zone. The "zoomed" views of the band gaps for both crystals clearly illustrate this difference. Since both energy gaps are indirect, the phonon contribution to the absorption processes should be important.

Composition of the calculated energy bands can be resolved with the help of partial density of states (PDOS) and total density of states (DOS) diagrams. Figs. 3 and 4 show the PDOS and total DOS for $ZnAl_2S_4$ and $ZnGa_2O_4$, respectively. These diagrams allow concluding that the conduction band in $ZnAl_2S_4$ is about 5 eV wide and is formed by the Al 3s and 3p states, which are hybridized with the S 3p states and Zn 4s, 4p states. The valence band is wide – about 7 eV – and consists of two sub-bands, clearly seen in the band structure as well: the upper one (between -6 and 0 eV) is a mixture of the S 3p states and Al 3s, 3p states. The lower one is narrow (between -7 and -6 eV) and is due to the completely filled Zn 3d states. Another band between -14 and -11 eV is created by the S 3s states with a minor contribution coming from the Al 3s, 3p states as well.

The conduction band in $ZnGa_2O_4$ is considerably wider (about 7 eV) than in $ZnAl_2S_4$ and is composed of Zn 4s, 4p states, Ga 4s, 4p states and O 2p states. The valence band is somewhat narrower in $ZnGa_2O_4$ (about 6 eV in comparison with 7 eV in $ZnAl_2S_4$) and does not exhibit any sub-band structure. 4s states of Ga occupy the bottom of the valence band, whereas the rest of the valence band consists of the Zn 3d states and O 2p states. Two remaining narrow bands at low energies are due to the Ga 3d states (at about -12.5 eV) and O 2s states (between -18 eV and -16 eV). It is also

noticeable that the Zn 3d states in $ZnGa_2O_4$ are spread over a wider region (almost 6 eV), whereas in $ZnAl_2S_4$ the Zn 3d states are localized in vicinity of -7 eV, at the very bottom of the valence band.

One of the main optical characteristics of a solid is its complex dielectric function $\varepsilon(\omega) = \varepsilon_1 + i\varepsilon_2$. The imaginary part $\varepsilon_2 = \mathrm{Im}(\varepsilon)$ of dielectric function is calculated in CASTEP numerically by a direct evaluation of the matrix elements between the occupied and unoccupied electronic states. The real part $\varepsilon_1 = \mathrm{Re}(\varepsilon)$ of $\varepsilon(\omega)$ is calculated then using the Kramers-Kronig transform. Such an approach, of course, has certain limitations. First of all, the local field effects (related to the fact that the electric field experienced at a particular site of a crystal lattice is screened by the polarizability of the atom at this site) are neglected. Also phonon contributions to the optical spectra, which are especially important for the crystals with indirect band gap, are also not taken into account, when calculating optical properties in CASTEP. However, even with these limitations the calculated spectra give reasonable agreement with experimental results (see, for example, calculations of absorption spectra for $PbWO_4$ [22, 23], TiO_2 [24] etc).

The dielectric functions for $ZnAl_2S_4$ and $ZnGa_2O_4$ are shown in Figs. 5 and 6, respectively. The instrumental smearing of 0.2 eV was used to model the broadening effects. The regions, in which the imaginary part ε_2 is different from zero, can be related to the absorption spectrum (which, in this case, will be due to the electronic transitions from the valence band to the conduction band). So, from these figures absorption starts at about 3 eV for $ZnAl_2S_4$ and 4 eV for $ZnGa_2O_4$, in agreement with the band gap estimations. The real part of $\varepsilon(\omega)$ in the limit of zero energy (or infinite wavelength) is equal to the square of the refractive index *n*. From Figs. 5 and 6 it is possible to estimate the value of *n* to be 2.24 for $ZnAl_2S_4$ and 1.65 for $ZnGa_2O_4$. Unfortunately, no experimental values of the refraction index were found in the literature, so these estimations remain to be purely theoretical.

Difference in electronic and band structure of these two compounds is also manifested in different shapes of the imaginary part of the dielectric function. Different band gaps are obviously related to different absorption edges. Besides, the widths of non-zero part of imaginary component of dielectric functions (in other words, the total width of the absorption spectra) are also different. It is directly linked with the widths of the conduction bands: a wider conduction band in $ZnGa_2O_4$ corresponds to a more extended absorption spectrum. In addition, a greater number of absorption peaks in $ZnGa_2O_4$ can be attributed to more significant contribution of the Zn 3d states to the total absorption, since they are distributed almost over the whole valence band (in $ZnAl_2S_4$ they are localized at the bottom of the valence band).

A further insight into the electronic properties of these compounds and chemical bond formation can be gained by considering the charge densities distributions (Figs. 7 and 8; one primitive cell is shown). As seen from these figures, in $ZnAl_2S_4$ there is strong hybridization between the S and Zn

atoms, whereas interaction between the Al and S atoms is not that pronounced. On the contrary, in $ZnGa_2O_4$ oxygen atoms interact strongly with both Zn and Ga atoms as well.

Different character of charge density distributions can be also seen in different values of the Mulliken charges [25] for ions in both compounds. They are as follows: Zn (+0.96), Ga (+1.22), O (–0.85) in $ZnGa_2O_4$ and Zn (+0.79), Al (+0.72), S (–0.56) in $ZnAl_2S_4$. Increased positive value of the Mulliken charge for Zn ions in $ZnGa_2O_4$ can be attributed to the stronger mixture with surrounding oxygen ions, when the negative charge is shifted towards oxygen ions, thus resulting in a greater absolute value of the anion's (oxygen) charge as well, when compared with that of sulfur in $ZnAl_2S_4$. This is also in line with a shorter calculated Zn – O distance (1.99713 Å) in comparison with Zn – S separation of 2.35347 Å. Additional confirmation of the obtained result can be based on the optical electronegativities of oxygen and sulfur ions, which would enhance covalency when going from O^{2-} to S^{2-} ligands [26].

3.2. Elastic properties and pressure effects

Elastic properties of cubic crystals are described by three independent elastic moduli C_{11}, C_{12}, C_{44} [27], with the following identities $C_{11} = C_{22} = C_{33}$, $C_{12} = C_{23} = C_{31}$, $C_{44} = C_{55} = C_{66}$. Calculations of these constants were performed for zero-th external pressure and optimized crystal structures; the results are shown in Table 2. For both compounds the values of the C_{11} constant are approximately 2-2.2 times greater than each of two remaining constants, which is in line with a well-known observation that for cubic crystals elastic constants decrease with increase of the lattice parameter [27]. It is also easy to notice that all elastic constants for $ZnAl_2S_4$ are about twice as small as those for $ZnGa_2O_4$, suggesting that the same external pressure should produce greater deformations in the former host.

Variations of the interionic distances with external hydrostatic pressure were studied by optimizing crystal structures for both considered crystal in the pressure range from 0 to 50 GPa. Fig. 9 shows the relative y/y_0 variation of the Ga–O, Zn–O distances in $ZnGa_2O_4$ and Al–S, Zn–S distances in $ZnAl_2S_4$ crystals (y stands for the interionic distance at some pressure P, whereas y_0 is the same distance at ambient pressure). The Ga–O chemical bond appears to be the stiffest, whereas the Zn–S bond is the weakest among the four considered ones.

Relative variations of these interionic distances were approximated by the quadratic least-squares fits $y/y_0 = a + b_1 P + b_2 P^2$. Approximation functions are plotted by solid lines in Fig. 9; they excellently follow the calculated values shown by different symbols for each chemical bond. The values of the approximation coefficients are listed in Table 3. They can be readily used for estimations

of the interionic distances for any arbitrary pressure up to 50 GPa, which is especially important for doped crystals, when the pressure dependent luminescence of dopants is studied.

Dependence of volume V on pressure P for solids can be modeled by the Murnaghan equation [28]

$$\frac{V}{V_0} = \left(1 + B_0' \frac{P}{B_0}\right)^{-\frac{1}{B_0'}} \quad (1)$$

where V_0 is the volume at ambient pressure, B_0 and B_0' are the bulk modulus and its pressure derivative, respectively. The V/V_0 ratios for unit cells of both crystals were calculated for pressures 0, 10, 20, 30, 40, and 50 GPa (Fig. 10, symbols). The least-squares fits to Eq. (1) are shown in Fig. 10 by solid lines. From these approximations, the values of B_0 and B_0' for $ZnAl_2S_4$ are 78.91 ± 0.47 GPa and 3.97 ± 0.04, respectively and for $ZnGa_2O_4$ 163.46 ± 1.31 GPa, 4.40 ± 0.09, accordingly. The extracted from the plots values of the bulk moduli B_0 are very close to those obtained as the results of the elastic constants calculations (Table 2). Estimated pressure derivatives of the bulk moduli are also within the typical range for solids. It is easy to note from Table 2 that the Cauchy condition for cubic crystals $C_{12} = C_{44}$ [29] is practically fulfilled. S. Haussühl [30] formulated that exactly this relation holds true for atoms, which interact only by central forces. It has been also noted [30-32] that $C_{12} - C_{44} < 0$ (negative Cauchy pressure) for covalent compounds and $C_{12} - C_{44} > 0$ (positive Cauchy pressure) for mostly ionic compounds. Application of the last two conditions to the data from Table 2 leads to the conclusion that $ZnAl_2S_4$ is a mostly covalent crystal, whereas $ZnGa_2O_4$ can be described in terms of more ionic bonds. It is also worthwhile to note here that another relation $C_{44} = (2C_{11} - C_{12})/3$ has been suggested in Ref. [33] as a better replacement for the $C_{12} = C_{44}$ condition. Indeed, it works almost perfectly for $ZnAl_2S_4$ and somewhat worse for $ZnGa_2O_4$.

Dependence of the calculated band gaps for both compounds on pressure is presented in Fig. 11. Linear fits (also shown in the Figure) describe well the behavior of the calculated band gaps. However, the value of E_g increases with pressure for $ZnGa_2O_4$ and exhibits opposite behavior for $ZnAl_2S_4$. Usually, band gaps increase with pressure, which also can be interpreted in terms of a blue shift of charge transfer transitions (which are, in other words, band-to-band transitions) with applied hydrostatic pressure [34]. Nevertheless, examples of decreased band gaps with applied pressure have been reported for a number of compounds: PbS [35], Li_3N [36], BN nanotubes [37], $MnIn_2S_4$ [38], $Li_4CaB_2O_6$ [39]. The reason for such a behavior can be either a high covalency of chemical bond, or significant re-distribution of electron density in the space between atoms [39]. Speaking about the crystals considered in the present paper, it can be mentioned that $ZnAl_2S_4$ is a more covalent compound than $ZnGa_2O_4$, with a quite considerable contribution of the sulfur ions into the conduction bands (hybridization with Zn and Al ions), which falls in line with some of the above given examples.

Finally, variation of the chemical bonds lengths with pressure should affect the charge densities distributions as well. Figs. 12 and 13 show how the charge density distributions are modified at the highest considered pressure of 50 GPa for $ZnAl_2S_4$ and $ZnGa_2O_4$, respectively (these figures should be compared with Figs. 7 and 8; in all figures one primitive cell is depicted for the sake of simplicity). Enhanced interactions in the Zn–O, Ga–O, Zn–S pairs are clearly seen form the shown contour plots.

It is also interesting to follow dependence of the Mulliken charges on pressure, which is represented in Table 4. In $ZnGa_2O_4$ the absolute values of the oxygen and gallium Mulliken charges are increasing with pressure, whereas the zinc Mulliken charge is decreasing. Such a result can be interpreted as re-distribution of the electron densities between these ions, namely, a shift of the electron density (negative charge) from gallium ions towards oxygen ions and from oxygen ions towards zinc ions, with the former shift dominating over the latter one.

In $ZnAl_2S_4$ the absolute values of the Mulliken charges for all three ions are decreasing, which can be thought of as a shift of electron density (negative charge) from sulfur ions towards zinc and aluminum ions. Additional information about the nature of the chemical bond between atoms can be extracted by using the concept of the Mulliken bond order. Although the absolute values of the bond order depend on the choice of the basis set, and thus their validity should not be overestimated [40], their *relative* values, calculated consistently for similar or even identical systems under various external conditions, like pressure, for example, can reveal some trends in behavior of particular chemical bonds and ions involved into their formation. A greater value of this parameter indicates the covalent character of the considered bond, whereas lower values of the bond order stress the ionic nature of the bond [40]. Analysis of the calculated Mulliken bond orders (Table 5) indicates that the Ga – O bond is the most ionic, whereas the Zn – S bond is the most covalent. On average, chemical bonds in $ZnAl_2S_4$ are more covalent than in $ZnGa_2O_4$ – this conclusion is also in line with the results of elastic constants estimations. Increase of pressure leads to a monotonic increase of the bond order (increased covalency) for each individual bond.

The results of calculation of the elastic constants can be used further to estimate one of the most important thermal characteristics of the studied compounds, the Debye temperature θ_D. This parameter is very important for an analysis of the specific heat, thermal conductivity and melting temperature. It can be estimated in the framework of the Debye-Grüneisen model by means of the following simple equation [41]

$$\theta_D = \frac{h}{k}\left[\frac{3n}{4\pi}\left(\frac{N_A\rho}{M}\right)\right]^{1/3} v_m, \qquad (2)$$

where h and k are the Planck's and Boltzmann's constants, respectively, N_A is the Avogadro's number, ρ is the crystal's density, M is the molecular weight, n denotes the number of atoms per unit cell (56

for both studied compounds), v_m is the mean sound velocity expressed in terms of the longitudinal v_l and transversal v_t sound velocities as follows:

$$v_m = \left[\frac{1}{3} \left(\frac{2}{v_t^3} + \frac{1}{v_l^3} \right) \right]^{-1/3} . \quad (3)$$

The v_l and v_t sound velocities are calculated as [42–44]

$$v_l = \sqrt{\frac{3B + 4G}{3\rho}} , \; v_t = \sqrt{\frac{G}{\rho}} , \quad (4)$$

with B being the bulk modulus and $G = \frac{G_V + G_R}{2}$ the isotropic shear modulus, which is calculated as the average value of the Voigt's shear modulus G_V (an upper limit for G values) and the Reuss's shear modulus G_R (a lower limit for G values). Analytical expressions for G_V and G_R are as follows:

$$G_V = \frac{C_{11} - C_{12} + 3C_{44}}{5} , \; \frac{5}{G_R} = \frac{4}{C_{11} - C_{12}} + \frac{3}{C_{44}} , \quad (5)$$

and the values of the elastic constants C_{11}, C_{12}, C_{44} are given in Table 2.

The density of $ZnAl_2S_2$ is 3.29 g/cm^3 [45] and the corresponding value for $ZnGa_2O_4$ is 6.17 g/cm^3 [46].

A summary of calculated values obtained from Eqs. (2) – (5) is presented in Table 6.

The $ZnGa_2O_4$ shear moduli, like other elastic constants, are approximately twice as large as their $ZnAl_2S_4$ counterparts. Also the sound velocities for $ZnGa_2O_4$ are somewhat greater than for $ZnAl_2S_4$. The values of Debye temperature decrease with increasing the lattice constants and anion's atomic number and weight; therefore, the highest acoustic phonons frequency should be greater in $ZnGa_2O_4$.

4. Conclusion

The first-principles calculations of the structural, electronic, optical and elastic properties for $ZnAl_2S_4$ and $ZnGa_2O_4$ have been performed using the CASTEP module of Materials Studio package. Both crystals are characterized as indirect band compounds. Structure of the calculated energetic bands was analyzed using the partial density of states diagrams. Although the structure of both crystals is the same, their electronic, elastic and bonding properties are quite different. It was shown that the conduction band is considerably wider in $ZnGa_2O_4$, whereas the valence band is spread over a wider energy interval in $ZnAl_2S_4$. The Zn 3d states are localized at the very bottom of the valence band in $ZnAl_2S_4$, whereas the same Zn 3d states occupy practically the whole valence band in $ZnGa_2O_4$.

Special attention has been paid to pressure effects and their influence on the electronic and structural properties. Variations of the Ga – O, Zn – O, Al – S, Zn – S chemical bonds lengths with pressure were approximated by the quadratic functions of applied pressure. It was shown that the Ga – O bond is the stiffest, and the Zn – S is the weakest one. Dependencies of the unit cell volumes on

pressure were fitted by the Murnaghan equation of state; determined from these fits the bulk moduli for both compounds are very close to those obtained from available in CASTEP direct calculations of elastic constants.

Analysis of the chemical bonds in both crystals (with calculations of the Mulliken bond orders) showed $ZnAl_2S_4$ to be considerably more covalent than $ZnGa_2O_4$. In addition, chemical bonds in the tetrahedral complexes formed by Zn ions and its neighbors (oxygen or sulfur) are more covalent than the chemical bonds in the octahedral complexes formed by the (Ga,O) and (Al, S) ions. Detailed analysis of the applied hydrostatic pressure effects has shown that it not only decreases the interionic distances, but also causes considerable re-distribution of the electron density, which was confirmed by calculating effective Mulliken charges for different pressures and following different trends of their variation. Finally, the calculated elastic constants were used to estimate the sound velocities and Debye temperatures for both compounds.

Acknowledgment: The author thanks Prof. Ü. Lille (Tallinn University of Technology) for allowing to use the computational facilities and Materials Studio package. Financial support from Estonian Science Foundation (Grants No. 7456, JD69, 6999 and 6660) is also appreciated.

References

[1] N. Ueda, T. Omata, N. Hikuma, K. Ueda, H. Hizoguchi, T. Hashimoto, H. Kawazoe, Appl. Phys. Lett. 61 (1992) 1954.
[2] I. Broussell, E. Fortin, L. Kulyuk, S. Popov, A. Anedda, R. Corpino, J. Appl. Phys. 84 (1998) 533.
[3] Z. Mazurak, J. Cisowski, J. Heimann, A. Naterpov, M. Czaja, Chem. Phys. 254 (2000) 25.
[4] S.I. Klokishner, O.V. Kulikova, L.L. Kulyuk, A.A. Naterpov, A.N. Naterpov, S.M. Ostrovsky, A.V. Palii, O.S. Reu, A.V. Siminel, Opt. Mater. 31 (2008) 284.
[5] B.R. Jovanić, I. Broussell, B. Panić, B. Radenković, M. Despotović, Mat. Res. Bull. 45 (2010) 186.
[6] M.G. Brik, Eur. Phys. J. B 49 (2006) 269.
[7] M.G. Brik, N.M. Avram, C.N. Avram, J. Mater. Sci: Mater. Electron. 20 (2009) S30.
[8] L. Pisani, T. Maitra, R. Valenti, Phys. Rev. B 73 (2006) 205204.
[9] J.S. Kim, H.L. Park, G.C. Kim, T.W. Kim, Y.H. Hwang, H.K. Kim, S.I. Mho, S.D. Han, Solid State Commun. 126 (2003) 515.
[10] H. Naito, S. Fujihara, T. Kimura, J. Sol-Gel Sci. Technol. 26 (2003) 997.
[11] A. Bouhemadou, R. Khenata, Phys. Lett. A 360 (2006) 339.
[12] M. Wendschuh-Josties, H.S.C. O'Neill, K. Bente, G. Brey, Neues Jahrbuch fuer Mineralogie. Monatshefte 6 (1995) 273.
[13] H.J. Berthold, K. Koehler, R. Wartchow, Zeitschrift fuer Anorganische und Allgemeine Chemie 496 (1983) 7.
[14] M.D. Segall, P.J.D. Lindan, M.J. Probert, C.J. Pickard, P.J. Hasnip, S.J. Clark, M.C. Payne, J. Phys.: Condens. Matter 14 (2002) 2717.
[15] J.P. Perdew, K. Burke, M. Ernzerhof, Phys. Rev. Lett. 77 (1996) 3865.
[16] R. Pandey, J.D. Gale, S.K. Sampath, J.M. Recio, J. Am. Ceram. Soc. 82 (1999) 3337.
[17] J.M. Recio, R. Franco, A.M. Pandas, M.A. Blanco, L. Pueyo, Phys. Rev. B 63 (2001) 184101.
[18] S. **Güner, F. Yıldız, B. Rameev, B. Akta ,** J. Phys.: Condens. Matter **17 (2005)** 3943.
[19] S.K. Sampath, D.G. Kanhere, R. Pandey, J. Phys.: Condens. Matter **11 (1999)** 3635.
[20] J.P. Perdew, M. Levy, Phys. Rev. Lett. 51 (1983) 1884.

[21] Z.H. Levine, D.C. Allane, Phys. Rev. B 43 (1991) 4187.
[22] Liu Tingyu, Shen Jianqi, Zhang Qiren, Solid State Commun. 135 (2005) 382.
[23] Liu Tingyu, Shen Jianqi, Zhang Qiren, Zhuang Songlin, J. Lumin. 126 (2007) 239.
[24] R.Shirley, M. Kraft, O.R. Inderwildi, Phys. Rev. B 81 (2010) 075111.
[25] R.S. Mulliken, J. Chem. Phys. 23 (1955) 1833.
[26] C.K. Jorgensen, in Progress in Inorganic Chemistry, edited by S. Lippard (Wiley-Interscience, New York, 1970), vol. 12, p. 101.
[27] C. Kittel, Introduction to Solid State Physics, John Wiley and Sons, 8th edition, 2004.
[28] F.D. Murnaghan, Proc. Natl. Ac. Sci. 30 (1944) 244.
[29] N.F. Mott, H. Jones, The Theory of the Properties of Metals and Alloys, Dover Publications, Inc., 1958.
[30] S. Haussühl, Phys. Kondens. Mater. 6 (1967) 181.
[31] V.P. Mikhal'chenko, Phys. Solid State 45 (2003) 453.
[32] H. Ledbetter, A. Migliori, Phys. Stat. Solidi B 245 (2008) 44.
[33] F. Milstein, D. J. Rasky, Solid State Commun. 55 (1985) 729.
[34] M. Moreno, M.T. Barriuso, J.A. Aramburu, P. Garcia-Fernandez, J.M. Garcia-Lastra, J. Phys.: Condens. Matter 18 (2006) R315.
[35] Li Wei, Chen Jun-fang, Wang Teng, Physica B 405 (2010) 1279.
[36] Wei Li, Jun-fang Chen, Teng Wang, Physica B 405 (2010) 400.
[37] S.S. Coutinho, V. Lemos, S. Guerini, Phys. Rev. B 80 (2009) 193408.
[38] J. Ruiz-Fuertes, D. Errandonea, F.J. Manjon, D. Martinez-Garcia, A. Segura, V.V. Ursaki, I.M. Tiginyanu, J. Appl. Phys. 103 (2008) 063710.
[39] Zhang Hong, Tang Jin, Cheng Xin-Lu, Chin. Phys. Lett. 25 (2008) 552.
[40] M.D. Segall, R. Shah, C.J. Pickard, M.C. Payne, Phys. Rev. B **54 (1996)** 16317.
[41] O.L. Anderson, J. Phys. Chem. Solids 24 (1963) 909.
[42] E. Schreiber, O.L. Anderson, N. Soga, Elastic Constants and Their Measurements McGraw-Hill, New York, 1973.
[43] M.B. Kanoun, S. Goumri-Said, A.H. Reshak, Comput. Mater. Sci. 47 (2009) 491.
[44] C. Çoban, K. Çolakoğlu, E. Deligöz, Y. Ő Çiftçi, Comput. Mater. Sci. 47 (2010) 758.
[45] G.A. Steigmann, Acta Cryst. 23 (1967) 142.
[46] L. Wang, Z. Hou, Z. Quan, H. Lian, P. Yang, J. Lin, Mat. Res. Bull. 44 (2009) 1978.

Table 1. Crystal lattice constants *a* and unit cell volume *V* for $ZnGa_2O_4$ and $ZnAl_2S_4$ crystals

	$ZnGa_2O_4$						$ZnAl_2S_4$	
	Exp.[a]	Calc.[b]	Calc.[c]	Calc.[d]	Calc.[e]	Calc.[f]	Exp.[g]	Calc.[b]
a, Å	8.3342	8.4412	8.4063	8.38	8.174	7.977	10.009	10.0340
V, Å^3	578.884	601.468	594.039	588.480	546.140	507.597	1002.702	1010.235

[a]Ref. [12]; [b]This work; [c]Ref. [11]; [d] Ref. [16]; [e] Ref. [19]; [f] Ref. [17]; [g] Ref. [13]

Table 2. Calculated elastic constants (all in GPa, except for non-dimensional Poisson ratios). The values in parenthesis for $ZnGa_2O_4$ are the results of calculations from Ref. [11].

Compound	C_{11}	C_{12}	C_{44}	Bulk modulus B_0	Young Modulus	Poisson ratio
$ZnAl_2S_4$	112.42 ± 2.05	50.84 ± 3.08	59.63 ± 6.13	71.37 ± 2.17	80.75	0.3114
$ZnGa_2O_4$	249.45 ± 3.54 (228)	121.81 ± 0.95 (120)	115.50±2.45 (107)	164.36 ±1.34 (156)	169.52	0.3281

Table 3. Coefficients of quadratic approximations $y/y_0 = a + b_1P + b_2P^2$ (P is pressure in GPa) of relative bond changes y/y_0 for $ZnGa_2O_4$ and $ZnAl_2S_4$.

Bond	y_0, Å	a	b_1, GPa^{-1}	b_2, GPa^{-2}
Ga–O	2.01716	$0.99959\pm5.5999\times10^{-4}$	$-0.00155\pm5.26746\times10^{-5}$	$9.18547\times10^{-6}\pm1.01123\times10^{-6}$
Zn–O	1.99713	$0.99943\pm8.30818\times10^{-4}$	$-0.00226\pm7.81491\times10^{-5}$	$1.48713\times10^{-5}\pm1.50028\times10^{-6}$
Al–S	2.40852	0.99884 ± 0.00155	$-0.00285\pm1.45810\times10^{-4}$	$2.16545\times10^{-5}\pm2.79921\times10^{-6}$
Zn–S	2.35347	0.99784 ± 0.00282	$-0.00400\pm2.65208\times10^{-4}$	$3.40235\times10^{-5}\pm5.09137\times10^{-6}$

Table 4. Mulliken charges of individual ions in $ZnGa_2O_4$ and $ZnAl_2S_4$ as a function of external pressure

Pressure,	$ZnGa_2O_4$			$ZnAl_2S_4$		
GPa	Zn	Ga	O	Zn	Al	S
0	0.96	1.22	– 0.85	0.79	0.72	– 0.56
10	0.93	1.25	– 0.86	0.79	0.72	– 0.56
20	0.91	1.27	– 0.86	0.78	0.71	– 0.55
30	0.90	1.29	– 0.87	0.77	0.70	– 0.54
40	0.90	1.30	– 0.88	0.76	0.70	– 0.54
50	0.89	1.32	– 0.88	0.76	0.69	– 0.53

Table 5. Mulliken bond orders for different chemical bonds in $ZnGa_2O_4$ and $ZnAl_2S_4$ as a function of external pressure

Pressure,	$ZnGa_2O_4$		$ZnAl_2S_4$	
GPa	Zn – O	Ga – O	Zn – S	Al – S
0	0.43	0.27	0.50	0.45
10	0.45	0.29	0.58	0.47
20	0.47	0.30	0.61	0.49
30	0.48	0.31	0.64	0.50
40	0.49	0.33	0.67	0.52
50	0.50	0.34	0.70	0.53

Table 6. Calculated shear moduli, sound velocities and Debye temperatures for $ZnAl_2S_4$ and $ZnGa_2O_4$

Compound	G_V, GPa	G_R, GPa	G, GPa	v_l, m/s	v_t, m/s	v_m, m/s	θ_D, K
$ZnAl_2S_4$	48.09	43.37	45.73	6342.4	3728.4	4132.5	943.8
$ZnGa_2O_4$	94.83	87.24	91.04	6805.2	3841.2	4272.6	1170.8

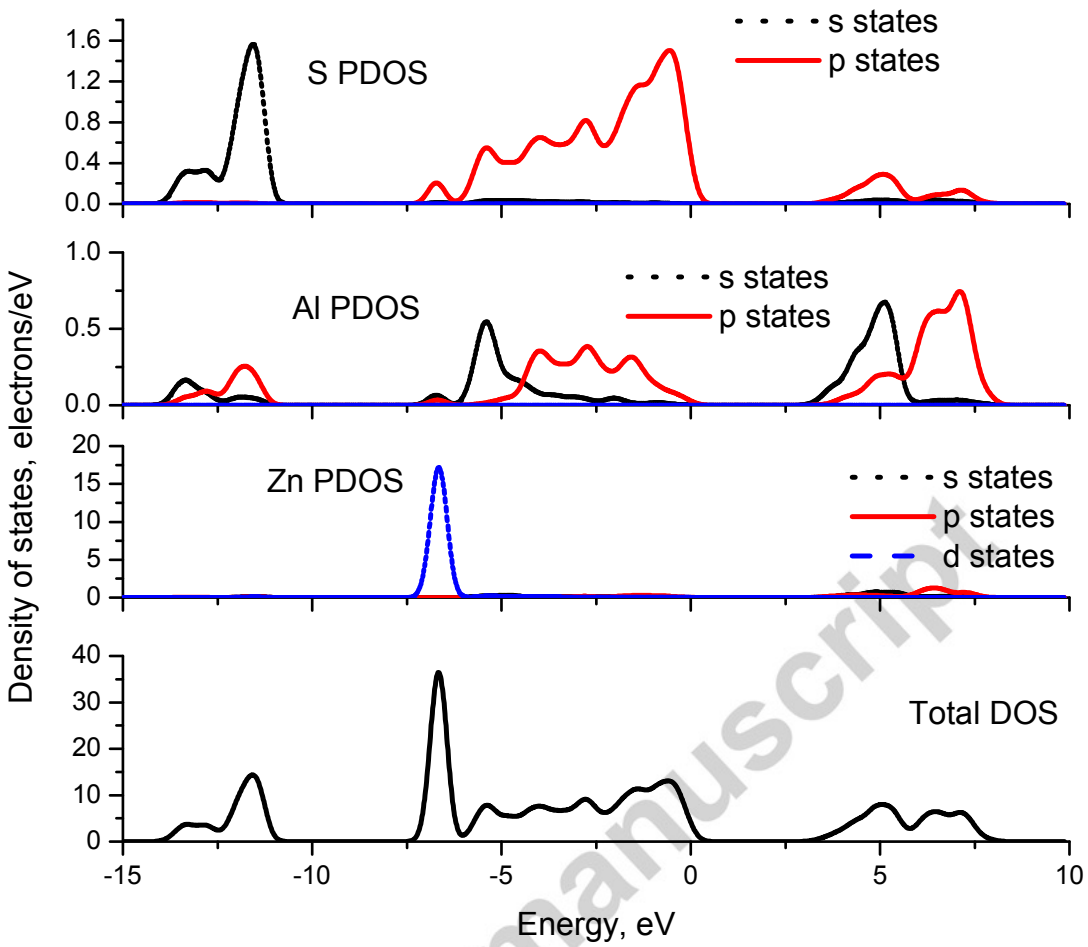

Fig. 3. Partial and total densities of states for $ZnAl_2S_4$. From top to bottom: sulfur, aluminum, zinc PDOS and total DOS.

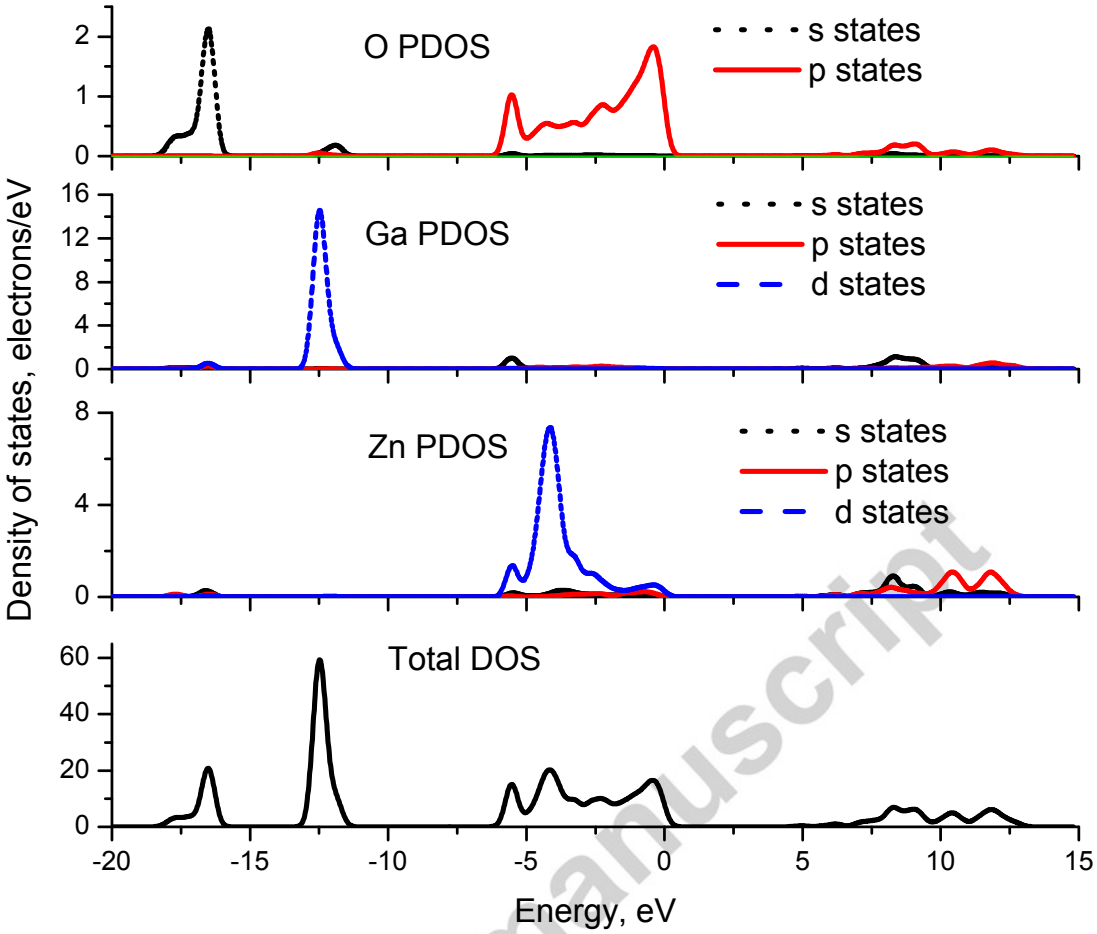

Fig. 4. Partial and total densities of states for $ZnGa_2O_4$. From top to bottom: oxygen, gallium, zinc PDOS and total DOS.

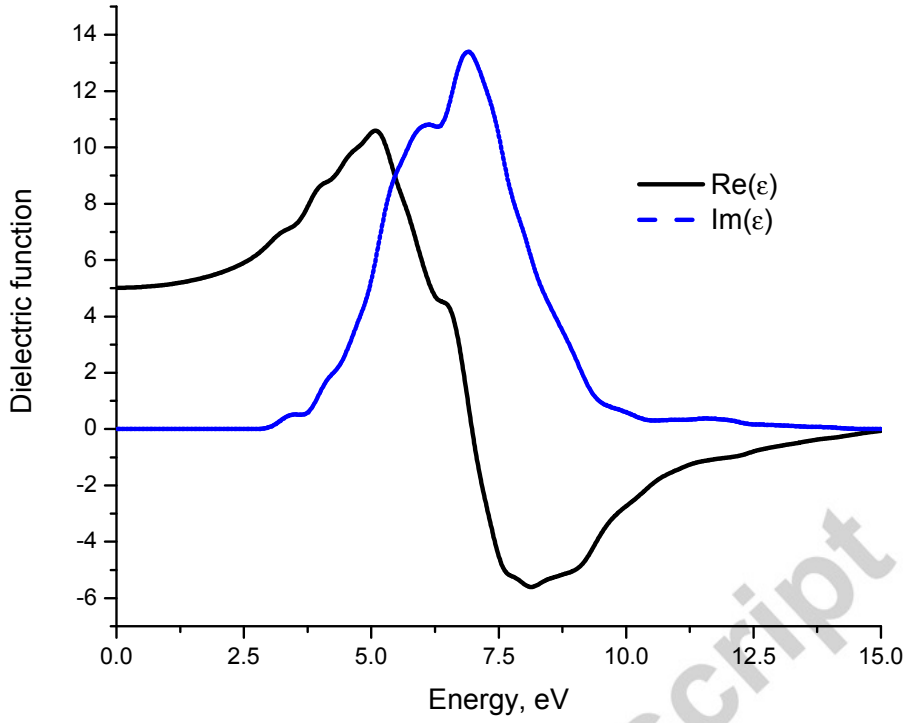

Fig. 5. Calculated dielectric function of $ZnAl_2S_4$.

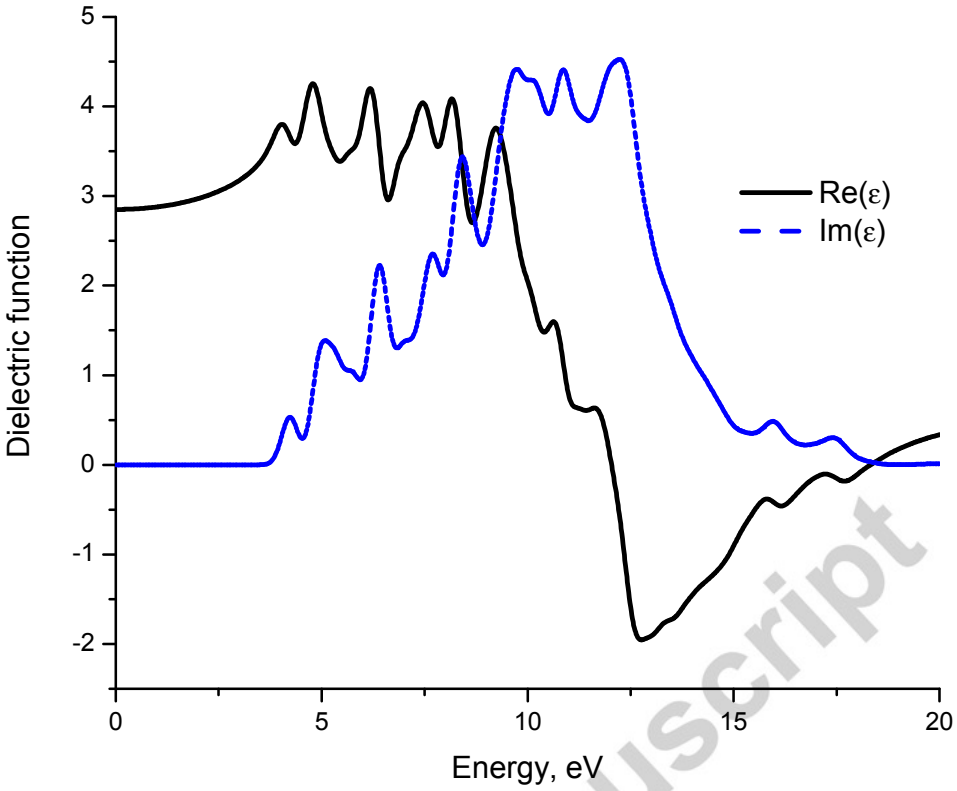

Fig. 6. Calculated dielectric function for $ZnGa_2O_4$.

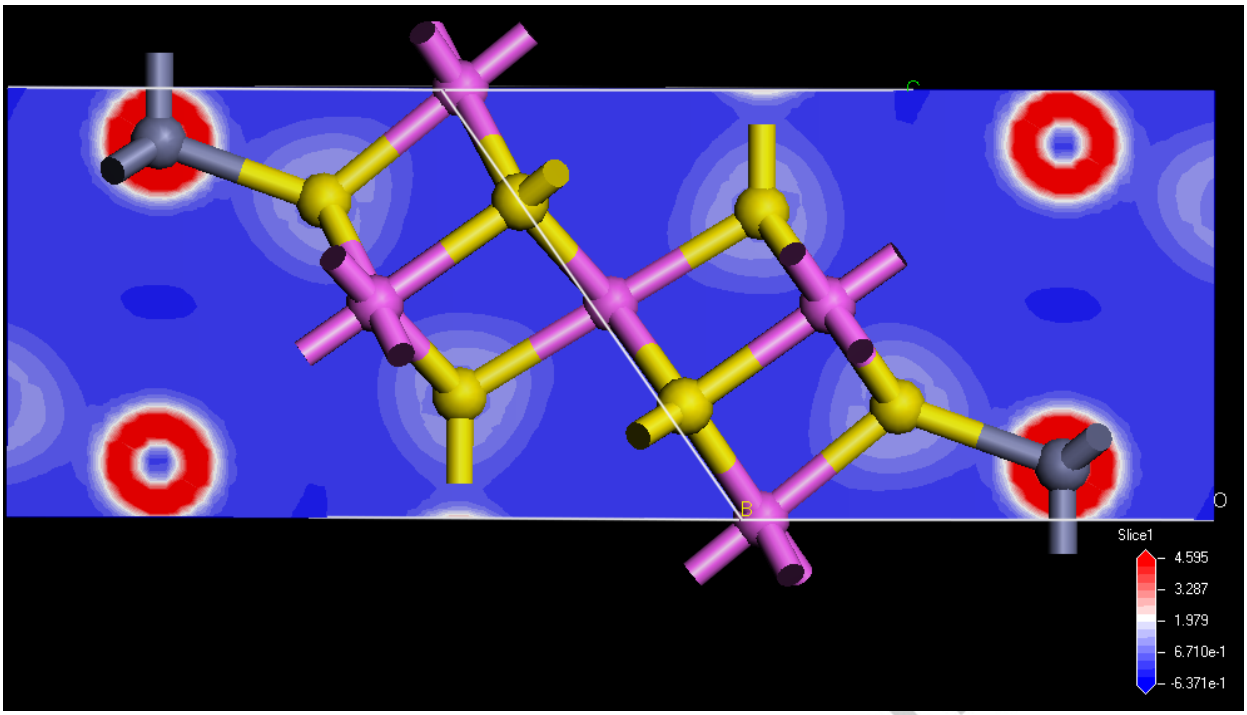

Fig. 7. A contour plot of the charge-density distribution in $ZnAl_2S_4$ (a normal to the shown slice is [0.707, -0.707, 0.000])

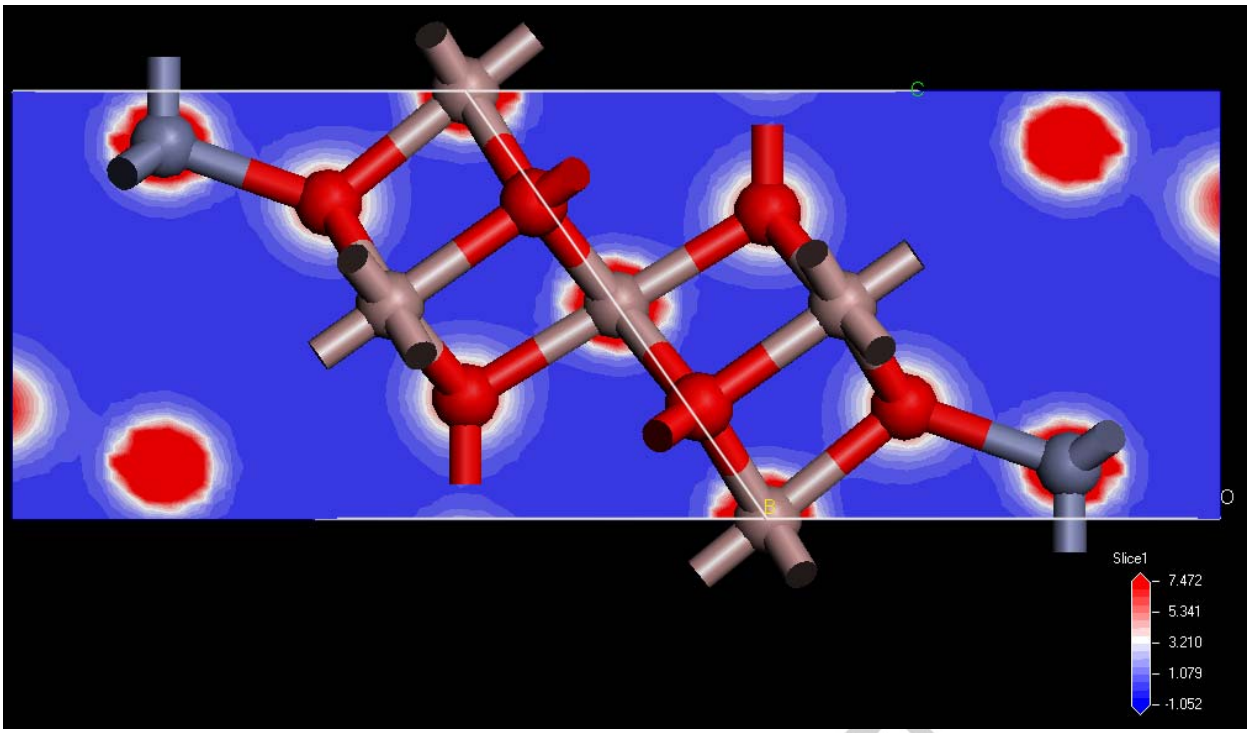

Fig. 8. A contour plot of the charge-density distribution in $ZnGa_2O_4$ (a normal to the shown slice is [0.707, -0.707, 0.000])

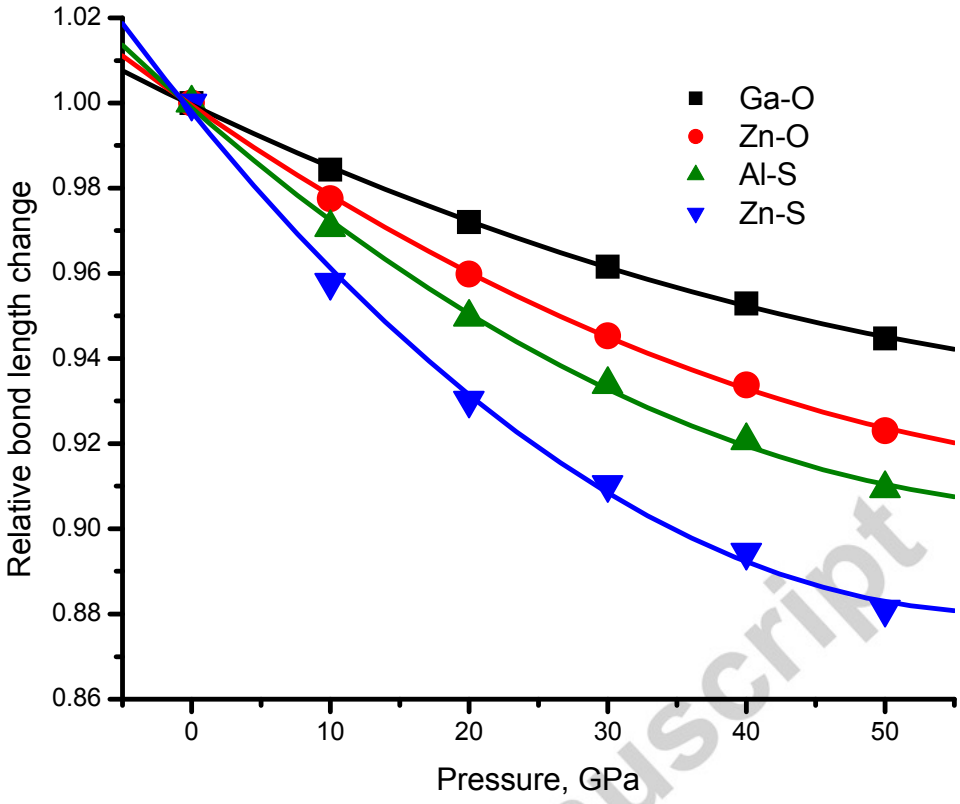

Fig. 9. Relative bond length changes for $ZnGa_2O_4$ and $ZnAl_2S_4$. The calculated values are shown by symbols, and the quadratic approximations (Table 3) are shown by solid lines.

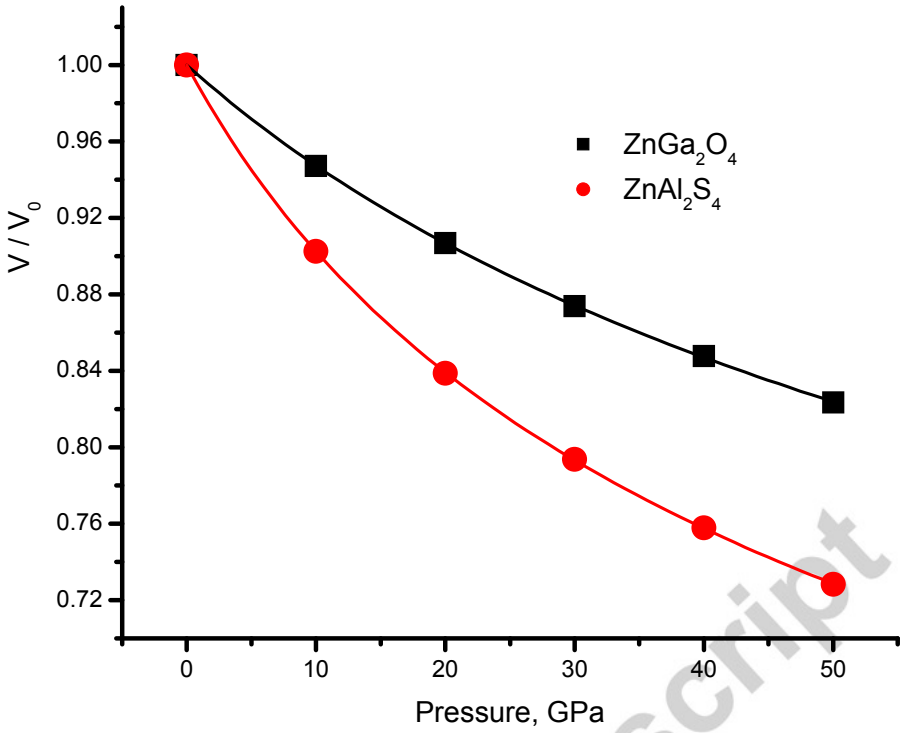

Fig. 10. Dependence of relative change of volume on pressure for $ZnGa_2O_4$ and $ZnAl_2S_4$. The calculated values are shown by symbols, and the fits to the Murnaghan equation (1) by solid lines.

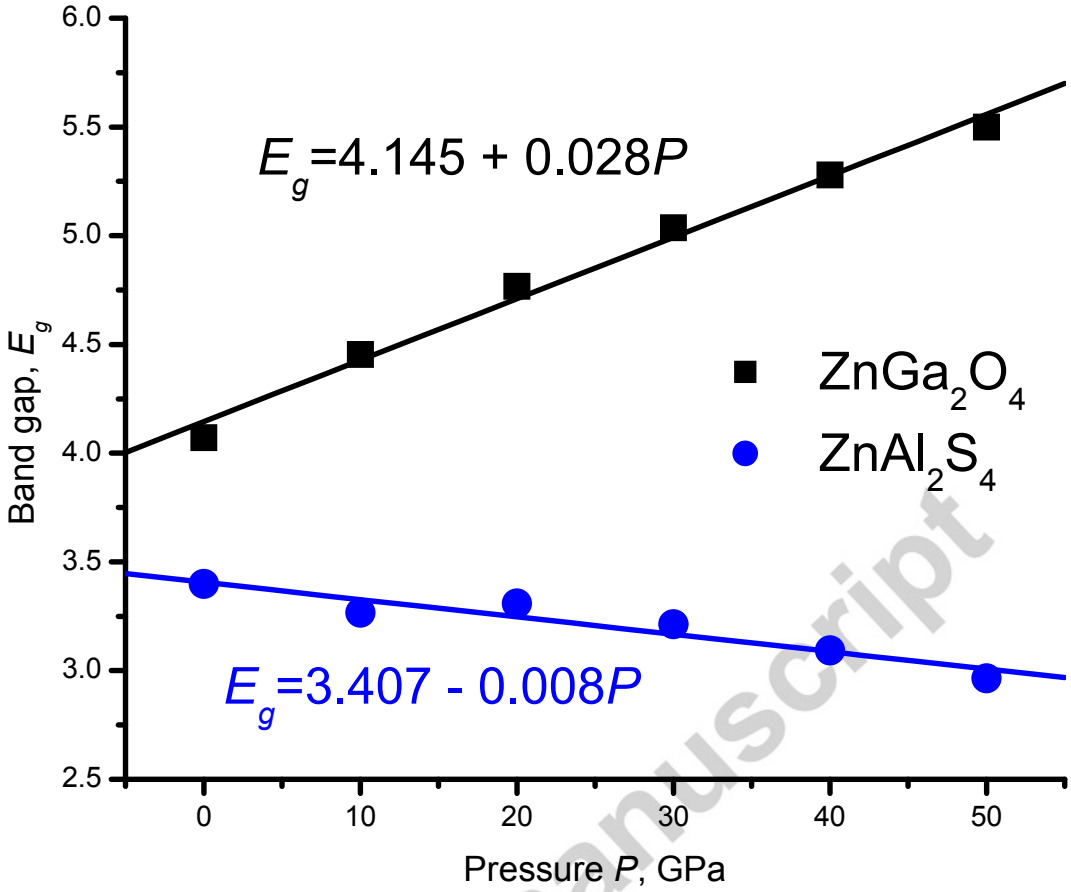

Fig. 11. Pressure dependence of the calculated band gaps E_g for $ZnGa_2O_4$ (squares) and $ZnAl_2S_4$ (circles). Linear fits and their equations are also shown.

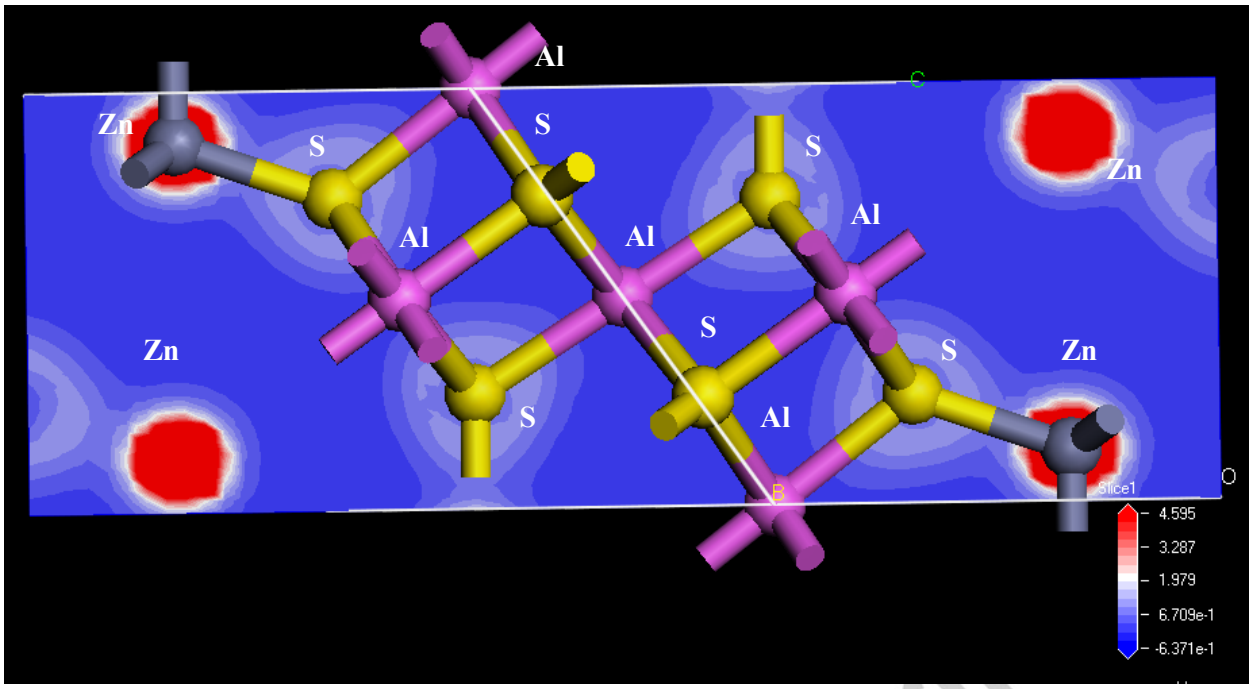

Fig. 12. A contour plot of the charge-density distribution in $ZnAl_2S_4$ (a normal to the shown slice is [0.707, -0.707, 0.000]; pressure 50 GPa)

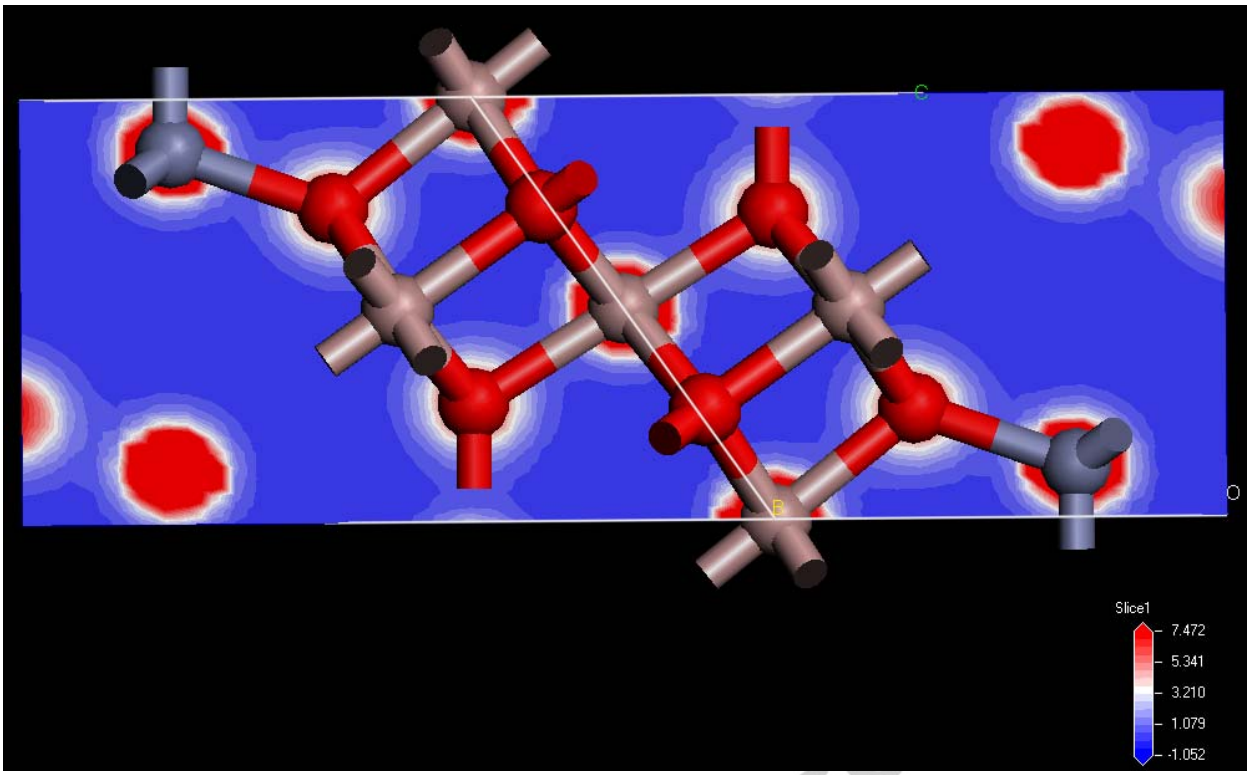

Fig. 13. A contour plot of the charge-density distribution in $ZnGa_2O_4$ (a normal to the shown slice is [0.707, -0.707, 0.000]; pressure 50 GPa)